Comparison of Anatomically-Defined Versus Physiologically-Based Regional Localization: Effects on PET-FDG Quantitation

Susan M. Resnick, Joel S. Karp, Bruce Turetsky and Raquel E. Gur

Laboratory of Personality and Cognition, GRC/NIA, Baltimore, Maryland and Departments of Psychiatry and Radiology, University of Pennsylvania, Philadelphia

The potential of anatomic imaging to improve the quantitative accuracy of functional brain imaging through refined regional definition is widely accepted. However, there are little data addressing the impact of approach to regional localization on quantitation of metabolic images in the absence of gross structural pathology. We compared MRI-based versus PET-based approaches to the analysis of PET ^{18}F-fluorodeoxyglucose (FDG) images using a standard adjustable template based on simple geometric regions. For the MRI-based approach, templates and individual regions were adjusted to each individual's anatomy, whereas the PET-based definition involved only global proportional adjustment of the standard templates. Metabolic rates for glucose and volume-to-whole brain ratios were determined by two operators for 78 volumes of interest in five subjects. Pairwise correlations indicated high interoperator agreement for each approach and high intraoperator agreement for MRI-based versus PET-based metabolic values. The stability of the metabolic rates and ratios among operators and analysis approaches was supported by low coefficients of variation across measurements and small average differences in paired comparisons. Thus, within the current spatial resolution of PET imaging, quantitation of metabolic images is relatively robust to image analysis approach in the absence of gross structural abnormality. To take advantage of the greater quantitative accuracy promised by high-resolution anatomic and functional imaging, more refined delineation of anatomic images will be necessary.

J Nucl Med 1993; 34:2201–2207

Accurate quantification of regional brain physiology with PET ultimately depends upon accurate localization of regions of interest (ROIs). Methods for the definition of PET ROIs fall broadly into two categories: physiology-based versus anatomy-based approaches. Early physiologic schemes involved placement of ROIs on "hot spots" or areas of increased radioactivity concentrations on PET scans. Subsequent approaches were based on templates developed from sectioned brains (*1*), published atlases or stereotactic definition of ROIs (*2,3*). More recently, it has become feasible to perform routine anatomic imaging in parallel with physiologic studies to define ROIs, which are then overlaid and/or co-registered with the physiologic images for quantification (*4–6*).

The use of an anatomically based system for ROI definition has a great deal of intrinsic appeal and is essential in the presence of gross structural pathology. However, with the current spatial resolution of PET imaging, the benefits obtained by individualizing template-based ROI definitions to each subject's anatomy in the absence of gross pathology are unclear. There are little data comparing this labor-intensive approach to a simpler method based on proportional adjustment of standard templates directly upon the physiologic images.

The present study was designed to examine the stability of PET quantitation across a number of approaches to image analysis. The following questions were addressed:

1. What is the interoperator reliability of a template system for ROI definition and quantitation?
2. How does anatomically based ROI localization compare with the use of a standard template overlaid directly on PET images?

MATERIALS AND METHODS

Subjects

The sample consisted of five research subjects from the Mental Health Clinical Research Center (MHCRC) on schizophrenia (*7*). Three subjects (2 male, 1 female) were patients with schizophrenia and two were normal volunteers (1 male, 1 female). The female control subject was subsequently excluded from further MHCRC evaluation due to information provided at follow-up that indicated a past history of substance abuse. Mean age was 26 ± 2.5 yr.

Measurements

MRI. MRI scans were obtained on a GE Signa 1.5 Tesla magnetic resonance scanner. Following a brief sagittal localizing scan, spin-echo images were acquired in the axial plane, with TR = 3000 and TE = 30/80, a slice thickness of 5 mm and no gap between slices. All scans received a clinical interpretation by experienced neuroradiologists. The scans of the two controls and the female

Received Oct. 29, 1992; revision accepted Aug. 5, 1993.

For correspondence or reprints contact: S.M. Resnick, PhD, GRC/NIA, Laboratory of Personality and Cognition, Room 2-C-14, 4940 Eastern Ave., Baltimore, MD 21224.

patient were read as normal. One male patient had a minimal increase in sulcal prominence for age, and the second male patient had multiple small punctate areas of abnormal signal, increased for age, in the white matter of the superior posterior parietal lobe.

PET. PET studies of regional cerebral glucose metabolism were performed using ^{18}F-fluorodeoxyglucose (FDG) and the PENN-PET scanner (*8*). Fluorine-18-FDG was injected as a bolus, and arterial blood samples were obtained over the next 90 min. A styrofoam headcast was made for each subject prior to radioisotope administration to aid in immobilization during scanning. Studies were performed under "resting conditions" with eyes and ears unoccluded. Following a 40-min uptake period, the subject was positioned in the PENN-PET scanner and the distribution of ^{18}F was imaged over the next 50 min. A laser beam mounted on the scanner was employed for head positioning to allow imaging along the canthomeatal axis.

Images were acquired in 2-mm slices, yielding a total of 45 transverse slices. To improve statistics, successive 2-mm sections were summed in an overlapping fashion to yield 43 slices of 6-mm thickness, with slice centers separated by 2 mm. The 2-mm axial sampling of the PENN-PET scanner is unique and minimizes the partial volume effect in the axial direction, leading to more accurate visualization and quantitation of resliced images (*9*). This is accomplished using large continuous detectors without plane-defining septa. These studies were acquired using the prototype PENN-PET scanner, which has an axial field of view of 9 cm. The relatively small field of view leads to some error in reslicing and regional quantitation because the entire brain is not imaged and all slices may not be available for particular volumes. The intrinsic transverse and axial resolution of the PENN-PET scanner is 5–6 mm FWHM, although the average resolution with reconstructive filtering is typically 7–8 mm. The finite spatial resolution limits the quantitation of small structures, as the partial volume effect will result in an underestimation of counts in a region.

Local cerebral metabolic rate for glucose (CMRglc) was determined as described previously (*10*) using experimentally determined values of the lumped constant and rate constants (*11*).

Image Analysis. PET image analysis was accomplished using the PETVIEW software package, developed by our PET group in collaboration with UGM Medical Systems. The software includes modules for image display in three orthogonal planes (transverse, sagittal, coronal), for reslicing in oblique planes and for ROI definition and quantification.

Template Development. We have developed a series of standard templates, which can be placed on either the MRI or PET images, using the PETVIEW software. Twenty-one templates have been defined in planes parallel to the anterior commissure-posterior commissure (AC-PC) line. The templates are separated by 4 mm along the z-axis and include 78 volumes, each volume including several ROIs from successive slices (see Table 2 for definition of volumes). ROI definition was guided by brain atlas sections and corresponding overlays (*12*) and by the Talairach and Tournoux brain atlas (*13*). Template regions were relatively simple geometric forms (Fig. 1), viewed as samples rather than inclusive of activity in particular structures. For each template, polygonal or elliptical regions were drawn on one hemisphere and then "mirrored" to the contralateral hemisphere, ensuring that ROIs were initially of identical size and orientation for the two hemispheres.

Template Implementation. MRI and PET images were reconstructed into volumes (a stack of transverse sections) and then each dataset was resliced parallel to the AC-PC line, using the

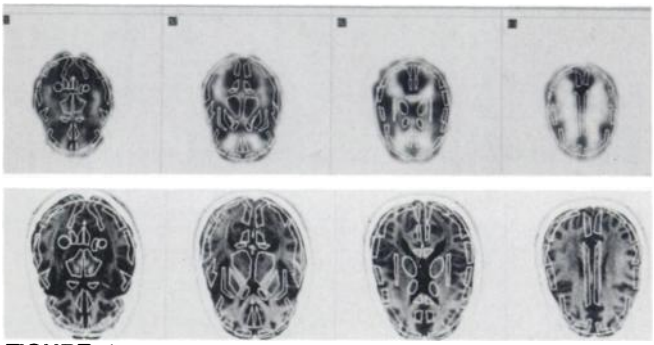

FIGURE 1. Adjusted template regions overlaid upon MRI (top) and corresponding PET (bottom) slices.

"oblique" software module. Since the PET image matrix consists of 2-mm^3 voxels, the interpolation errors are small and do not significantly affect the quantitation. The voxel size in the MRI image is typically 0.78 × 0.78 × 5 mm, which is fairly coarse in the axial direction but did not lead to difficulty in visualizing anatomic structures after reslicing. The AC-PC line was defined from the sagittal view and, following Talairach and Tournoux Methodology (*13*), cuts through the superior portion of the anterior commissure and the inferior portion of the posterior commissure. On the PET images, the AC-PC line was not clearly visible, but an approximation was provided by a line passing through the most anterior part of the frontal lobe, the anterior corpus callosum and the occipital pole (*14*). Alternate PET slices were processed, yielding quantification of approximately 21 slices with 4-mm spacing.

For the anatomically based ROI definition, the standard templates were first overlaid on the resliced MRI images. The most superior slice containing the caudate nucleus and overall fit were used as guides for positioning in the z-axis. The templates were customized to each individual's anatomy in three steps:

1. A global proportional adjustment for the whole template series was performed through translation, rotation and resizing.
2. Regions within each slice were adjusted proportionally as a group.
3. Individual ROIs were positioned over appropriate structures by translation, rotation and resizing.

These MRI-based templates were then overlaid upon corresponding PET slices, again using the most superior slice containing caudate nucleus as a guide for positioning in the z-axis. Due to scaling differences between our MRI and PET images, it was also necessary to globally resize each MRI-adjusted template slice to the resliced (AC-PC oriented) PET sections using the 50% threshold of the edge of the brain as a guide. From the resliced PET images, count densities were then determined for each region and regional cerebral glucose metabolism was quantified (*10,11*). Area-weighted average metabolic rates for glucose metabolism were computed across all slices to yield metabolic rates for the 78 volumes of interest. "Whole-brain" metabolism was estimated by an area-weighted average of metabolic rates for all regions. Because most of the volumes define gray matter structures, the whole brain value primarily reflects gray matter metabolism.

For the physiologically-based ROI definition and quantification, the original templates were placed directly upon the PET images. The head of the caudate nucleus and overall fit were again used as guides for positioning in the z-axis. The global atlas- and slice-based adjustments were performed using the 50% threshold

TABLE 1
Pairwise Correlations Among Measurements

	Operator 1		Operator 2		
	1. MRI	2. PET	3. MRI	4. PET	5. MRI-PET1*
Operator 1					
1. MRI-based	—	**0.98**	*0.96*	0.95	0.98
2. PET-based	**0.95**	—	0.96	*0.96*	0.98
Operator 2					
3. MRI-based	*0.92*	0.90	—	**0.98**	0.97
4. PET-based	0.90	*0.92*	**0.95**	—	0.96
5. MRI-based PET1*	0.96	0.95	0.93	0.91	—

*Operator 2's MRI-based template upon the resliced PET image of Operator 1.

Correlations for absolute CMRglc are above the diagonal and those for volume-to-whole brain ratios are below the diagonal. For clarity, interoperator correlations using the same approach are in italics, while intraoperator correlations between MRI-based versus PET-based approaches are in bold.

Number of paired observations varies between 339 and 365. All correlations are significant at $p = .0001$.

of the edge of the brain for placement of the outer regions, but ROIs were not manipulated individually. Count densities and CMRglc for glucose metabolism were determined as described above.

Procedures

Five measurements of metabolic activity were made for each subject's PET image:

1. Operator 1, MRI-based.
2. Operator 1, PET-based.
3. Operator 2, MRI-based.
4. Operator 2, PET-based.
5. Operator 2, MRI-based using the resliced PET image of Operator 1.

Thus, the first four measurements provide assessments of intraoperator agreement across MRI- and PET-based methods and interoperator agreement within and across methods. The fifth measurement was performed to evaluate the extent to which interoperator variability might be due to differences in reslicing the PET images versus fitting templates to the MRI.

Angle of reslicing, positioning of templates in the z direction and template manipulation varied between operators, allowing assessment of inter-rater reliability for the entire procedure. Since the purpose of the intraoperator comparisons of MRI- and PET-based quantitation was to evaluate the variability in metabolic rates as a function of template manipulation on anatomic versus physiologic images, positioning of the templates in the z direction and angle of reslicing were fixed within operators for these comparisons. These factors were also fixed across operators for the fifth measurement and were identical to those for the first and second measurements.

Statistical Analysis

All analyses were performed for absolute values of CMRglc and volume-to-whole brain ratios. Pairwise correlations among measurements were calculated across subjects and volumes to examine: interoperator agreement for a given approach (e.g., 1 versus 3, 2 versus 4), intraoperator agreement across MRI- and PET-based approaches (e.g., 1 versus 2, 3 versus 4) and the agreement between operators when using the same resliced PET image (1 versus 5). Variability in these values across measurements was examined by analysis of coefficients of variation. For each subject, coefficients of variation across the five measurements were calculated for each volume. These coefficients of variation were then averaged across subjects and across both subjects and volumes to provide, respectively, mean coefficients of variation for each volume and an overall mean value. Note that these values do not include variability in metabolism between subjects, and variability between subjects is reflected only to the extent that *agreement among measurements* differs between subjects. In addition, paired t-tests were performed to examine the magnitude, direction and consistency of differences between measurements. T-tests were done for the following comparisons: interoperator for MRI-based and PET-based values (1 versus 3, 2 versus 4), intraoperator for MRI-based versus PET-based values (1 versus 2, 3 versus 4) and between operators for the MRI-based approach using a fixed resliced PET image (1 versus 5).

RESULTS

Pairwise correlations among the five measurements are presented in Table 1. Correlations for absolute metabolic rates are above the diagonal and correlations for volume-to-whole brain ratios are below the diagonal. All correlations indicate significant and high agreement among measures. As expected, correlations for absolute values are higher than those for volume-to-whole brain ratios, because global metabolic differences between subjects contribute to the former. Scatterplots of intraoperator and interoperator correlations for volume-to-whole brain ratios are illustrated in Figure 2.

Mean coefficients of variation for the 78 volumes are presented in Table 2. The average volume size was 3.47 ± 4.9 cm^3, containing an average of 216.9 voxels (each $2 \times 2 \times 4$ mm). The volume sizes ranged from a mean of 0.07 cm^3 for the uncus to a mean of 26.8 cm^3 for the cerebellum. As described above in the statistical analysis section, the mean coefficients of variation reflect the average coefficients of variation across the five measurements and the five subjects. The mean ± s.d. coefficient of variation across all volumes was 6.1% ± 3.8% (range from 1.6% to 27.6%) for absolute values of CMRglc and 6.2% ± 4.1% (range from

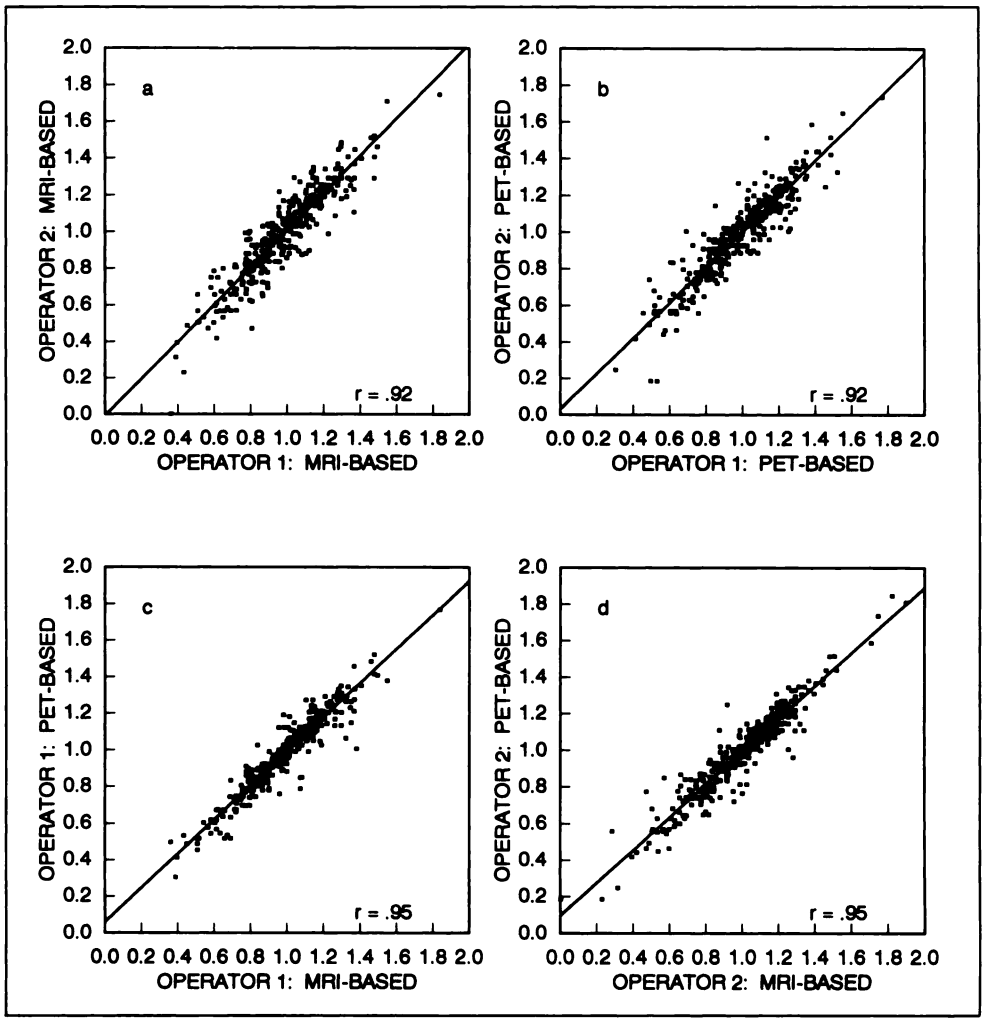

FIGURE 2. Scatterplots of correlations between measurements for volume-to-whole brain ratios.

1.3% to 28.8%) for volume-to-whole brain ratios. Six of the 78 coefficients of variation for absolute values and 9 of the ratio values are greater than 10%. With the exception of the medulla, which is subject to error due to reslicing with a 9-cm field of view acquisition, all volumes have coefficients of variation less than 15%. Note that smaller subcortical and limbic structures, including the basal ganglia, hippocampus, and amygdala, show a similar degree of stability across measures as do the larger cortical volumes.

As described above, differences in CMRglc and ratio values between pairs of measurements (1 versus 3, 2 versus 4, 1 versus 2, 3 versus 4, 1 versus 5) were examined to assess the consistency of the varied approaches to image analysis. Average paired differences across the 78 volumes for CMRglc and ratio values are presented in Table 3. There were small but consistent differences in absolute values of CMRglc across operators, reflecting slightly higher metabolic rates for Operator 1 compared with Operator 2. The average differences in CMRglc in Table 3 correspond to less than 2% of the mean CMRglc values. Note that corrections for partial volume effects, which we are not currently performing, would result in much greater increases in metabolic rates, but would affect all measurements. For volume-to-whole brain ratios, there were no significant differences between methods.

The t-test comparisons for individual volumes were performed for exploratory purposes, using a 0.01 level of significance due to the large number of tests and small number of observations. With this criterion, a maximum of 4 of the 78 volumes reached significance for each comparison of two measurements, but no particular volume emerged as more sensitive to the type of analysis.

DISCUSSION

Despite the increasing use of anatomically based measurements for localization of ROIs on functional images, there have been few attempts to directly evaluate the impact of different approaches to regional definition on quantitative results. The findings of the present investigation suggest that in the absence of gross pathology, image quantitation is relatively robust to the method of image analysis within the current resolution of PET. We observed high interoperator and intraoperator agreement using a standard template approach for MRI-based and PET-based approaches to image analysis. Correlations among measure-

TABLE 2
Mean Coefficients of Variation for 78 Volumes Across the Five Measurements and Five Subjects

	Absolute CMRglc		Volume-to-Whole brain ratio	
	Right	Left	Right	Left
1 Anterior cingulate	3.3	3.3	3.9	4.3
3 Superior frontal gyrus	3.9	4.0	3.0	3.0
5 Middle frontal gyrus	5.8	3.1	4.7	3.2
7 Sensorimotor cortex	8.8	2.0	7.7	2.2
9 Superior temporal gyrus	7.0	2.1	5.7	2.1
11 Supramarginal gyrus†	14.8	6.1	14.2	5.4
13 Corpus callosum anterior	6.6	7.2	6.5	6.6
15 Caudate nucleus	4.1	3.9	4.5	4.6
17 Insula	1.5	2.6	3.0	4.0
19 Thalamus	3.3	2.8	4.0	3.4
21 Lateral occipital cortex	6.6	5.3	5.6	4.8
23 Medial occipital cortex	5.7	5.4	5.1	4.7
25 Posterior cingulate gyrus	5.5	4.8	6.4	5.6
27 Corpus callosum posterior	10.2	10.0	10.3	10.5
29 Middle temporal gyrus	7.1	3.3	5.6	2.8
31 Inferior frontal gyrus	8.6	3.9	8.0	3.8
33 Globus pallidus*	1.3	2.2	2.5	1.6
35 Putamen	2.2	1.8	2.6	2.4
37 Parahippocampal gyrus	4.1	4.2	5.1	4.6
39 Hippocampus	6.8	2.9	6.3	3.1
41 Cerebellum	4.8	3.5	4.4	3.4
43 Midbrain	3.0	3.8	2.7	3.9
45 Orbital cortex	10.0	8.9	10.2	8.9
47 Gyrus rectus	6.5	5.7	7.3	6.4
49 Amygdala	4.8	3.0	4.8	4.1
51 Lingual gyrus	3.6	4.8	2.6	5.1
53 Lateral occipital-temporal gyrus	8.3	6.3	6.9	5.7
57 Hypothalamus	6.2	8.7	6.2	8.0
59 Uncus	6.7	12.2	7.4	11.8
61 Pons	8.4	5.9	7.4	5.7
63 Medulla‡	28.8	19.6	27.6	18.1
65 Cingulate gyrus (anterior + posterior)	12.5	4.6	12.0	4.2
67 Angular gyrus‡	6.3	6.5	5.1	6.1
69 Precuneus‡	6.4	3.4	7.3	2.8
71 Paracentral lobule‡	6.8	7.5	7.7	6.6
73 Superior frontal/Middle frontal†	5.8	4.1	5.9	4.6
75 Medial superior/Inferior parietal	9.7†	7.3	9.4†	8.3
77 Lateral superior/Inferior parietal§	8.5	9.7	8.3	10.1
79 Inferior temporal gyrus	8.3	5.2	7.3	5.0

*MRI-based volumes for Operator 1 only because Operator 2 was not confident of visualization of this volume on MRI.
†ROI imaged in four subjects.
‡ROI imaged in three subjects.
§ROI imaged in two subjects.

ments were high for both absolute metabolic rates and volume-to-whole brain ratios. The stability of image quantitation across measurements was confirmed by coefficients of variation of less than 10% for most volumes and average differences in paired comparisons of less than 2% for absolute metabolic rates and less than 1% for the volume-to-whole brain ratios. A variety of errors contributes to variability in quantitation, including accuracy of reslicing reconstructed images, positioning of templates in the axial direction and template manipulation. Despite these errors, our results suggest that individual differences in metabolism and in the regional distribution of metabolism can be measured reliably using a variety of relatively simple image analysis approaches.

While all correlations among methods were very high, the correlations for volume-to-whole brain ratios between MRI and PET-based measurements for each operator (0.95) tended to be higher than those between operators for a single method (0.92). This indicates that there is not a clear advantage with the MRI-based method compared to the PET-based method in the presence of other errors and the variability among trained operators. An unexpected finding was that relatively smaller subcortical and limbic structures, such as the basal ganglia, amygdala and hip-

TABLE 3
Average Differences in Metabolic Rates and Ratios Across Measures and Volumes

	Absolute CMRglc (mg/100 g · min^{-1})	Volume-to-Whole brain ratios
	Mean (s.d.)	Mean (s.d.)
Operator 1 vs. Operator 2		
MRI-based	0.07 (0.39)†	−0.006 (0.10)
PET-based	0.04 (0.36)*	−0.004 (0.09)
MRI based on Operator 1 resliced PET§	0.06 (0.26)‡	−0.003 (0.07)
MRI-based vs. PET-based		
Operator 1	0.02 (0.26)	0.007 (0.07)
Operator 2	−0.02 (0.29)	0.006 (0.08)

*$p < 0.05$; †$p < 0.01$; ‡$p < 0.001$.
§Operator 2's MRI-based template upon the resliced PET image of Operator 1. Number of volumes in each comparison ranges from 336 to 358.

pocampus, showed stability across operators and approaches comparable to that for the larger cortical volumes. The fact that our analyses were volume-based rather than slice-based was a likely contributor to this stability.

Although this study was based on a particular template system, the consistency of findings across measurements suggests these results may be general to similar systems implemented in many other PET facilities. The relative insensitivity of metabolic measures to variability in image analysis approach suggests that stereotactic methods should provide adequate estimation of region localization in normal individuals. However, the extent to which the findings can be generalized beyond FDG images is unclear, because proportional adjustment of the template slices on physiologic images requires a clearly defined brain contour.

The potential of anatomically-based ROI localization to improve quantitative accuracy was not fully tested in this study due to limitations in regional definition on MRI and the use of relatively simple geometric regions. The MRI-based measurements were limited by the ability to define boundaries of specific cortical gyri and limbic structures, e.g., hippocampus, from transverse sections, because this is notoriously difficult even for trained operators. In addition, simple geometric regions do not accurately describe convoluted structures such as cortical gyri and tap heterogeneous tissue composed of cerebrospinal fluid and white matter in addition to gray matter. Schmidt et al. (*15*) have recently described the errors introduced by tissue heterogeneities in determination of glucose metabolism using the current kinetic models of the FDG method. Thus, we believe that more refined regional localization on MRI, including use of lateral surface views of three-dimensional reconstructions for gyral definition, consideration of tissue heterogeneities and partial volume correction, will improve accuracy in quantifying functional images and lead to greater differences between anatomically based and physiologically based approaches to image analysis. While this is a future goal, the use of simple geometric regions and transverse images for regional localization is typical of the approach currently employed in many PET facilities. Our results offer an index of the potential error in applying standardized templates for PET quantitation in the absence of structural pathology.

Although the robustness of the quantitation of PET metabolic images is encouraging, we do not advocate abandonment of anatomically based approaches to ROI localization. The limits of tolerance to pathology of proportional adjustments of standard templates or stereotactic atlases are unclear. MRI-based ROI definition will be essential in the presence of gross structural abnormality and may be critical in identifying subtle abnormalities or changes in brain function across repeated studies. Difficulties in localizing subtle changes between repeated studies highlight the importance of anatomic measurement (*16*). Moreover, segmented MRIs can be used to estimate CSF and gray and white matter volumes for partial volume correction (*17,18*). These enhancements will be particularly important for conditions associated with brain atrophy, such as dementia and normal aging, where PET-based analysis is likely to underestimate specific regional metabolic rates due to confounding effects of tissue loss. To fully realize the greater quantitative accuracy promised by high-resolution anatomic imaging, refined methods for segmentation of tissue types and delineation of ROIs on structural images must be concurrent with improvements in the spatial resolution of PET imaging.

ACKNOWLEDGMENTS

This research was supported by NIMH grants MH 43740, MHCRC 43880, MH 48539, NIH grant NS 14867 and a Ben Franklin Partnership Foundation Grant. We thank Gerd Muehllehner, Shenji Guan and Manuel Angel for their efforts in the development of PETVIEW and the staffs of the PET and cyclotron facilities for their contributions in performing the PET scans.

REFERENCES

1. Dann R, Muehllehner G, Rosenquist A. Computer-aided data analysis of ECT data [Abstract]. *J Nucl Med* 1983;24:82.
2. Bohm C, Greitz T, Kingsley D, Berggren B, Ollson L. Adjustable computerized stereotaxic brain atlas for transmission and emission tomography. *AJNR* 1983;4:731–733.
3. Fox PT, Perlmutter JS, Raichle ME. A stereotactic method of anatomical localization for positron emission tomography. *J Comput Assist Tomogr* 1985;9:141–153.
4. Evans AC, Beil C, Marrett S, Thompson CJ, Hakim A. Anatomical functional correlation using an adjustable MRI based atlas with PET. *J Cereb Blood Flow Metab* 1988;8:813–830.
5. Evans AC, Marrett S, Torrescorzo J, Ku S, Collins L. MRI-PET correlation in three dimensions using a volume-of-interest (VOI) atlas. *J Cereb Blood Flow Metab* 1991;11:A69–A78.
6. Pelizarri CA, Chen GTY, Spelbring DR, Weichselbaum RR, Chen C-T. Accurate three-dimensional registration of CT, PET, and MR images of the brain. *J Comput Assist Tomogr* 1989;13:20–26.
7. Gur RE, Mozley PD, Resnick SM, et al. Magnetic resonance imaging in schizophrenia. I. Volumetric analysis of brain and cerebrospinal fluid. *Arch Gen Psychiatry* 1991;48:407–412.
8. Karp JS, Muehllehner G, Mankoff DA, et al. Continuous-slice PENN-PET:

a positron tomograph with volume imaging capability. *J Nucl Med* 1990;31: 617–627.
9. Karp JS, Daube-Witherspoon ME, Muehllehner G. Factors affecting accuracy and precision in PET volume imaging. *J Cereb Blood Flow Metab* 1991;11:A38–A44.
10. Reivich M, Kuhl D, Wolf AP, Greenberg J, et al. The ^{18}F-fluorodeoxyglucose method for the measurement of local cerebral glucose utilization in man. *Circ Res* 1979;44:127–137.
11. Reivich M, Alavi A, Wolf AP, et al. Glucose metabolic rate kinetic model parameter determination in man: the lumped constants and rate constants for ^{18}F-fluorodeoxyglucose and ^{11}C-deoxyglucose. *J Cereb Blood Flow Metab* 1985;5:179–192.
12. Gee JC, Reivich M, Bajcsy R. Elastically deforming 3D atlas to match anatomical brain images. *J Comput Assist Tomogr* 1993;17:225–236.
13. Talairach J, Tournoux P. *Co-planar stereotaxic atlas of the human brain: 3-dimensional proportional system: an approach to cerebral imaging.* New York: Thieme Medical Publishers, Inc.; 1988.
14. Friston KJ, Passingham RE, Nutt JG, Heather JD, Sawle GV, Frackowiak RSJ. Localisation in PET images: direct fitting of the intrecommissural (AC-PC) line. *J Cereb Blood Flow Metab* 1989;9:690–695.
15. Schmidt K, Lucignani G, Moresco RM, et al. Errors introduced by tissue heterogeneity in estimation of local cerebral glucose utilization with current kinetic models of the [^{18}F]fluorodeoxyglucose method. *J Cereb Blood Flow Metab* 1992;12:823–834.
16. Drevets WC, Videen TO, MacLeod AK, Haller JW, Raichle ME. PET images of blood flow changes during anxiety: correction. *Science* 1992;256: 1696.
17. Meltzer CC, Leal JP, Mayberg HS, Wagner HN Jr, Frost JJ. Correction of PET data for partial volume effects in human cerebral cortex by MR imaging. *J Comput Assist Tomogr* 1990;14:561–570.
18. Muller-Gartner HW, Links JM, Prince JL, et al. Measurement of radiotracer concentration in brain gray matter using positron emission tomography: MRI-based correction for partial volume effects. *J Cereb Blood Flow Metab* 1992;12:571–583.